Int J Adv Manuf Technol (2001) 17:196–203

The International Journal of
Advanced
Manufacturing
Technology

Laser Forming with Constant Line Energy

Wenchuan Li and Y. Lawrence Yao

Department of Mechanical Engineering, Columbia University, 220 Mudd Building, MC 4703, New York, NY 10027

This paper investigates the condition of constant line energy, that is, the ratio of laser power to scanning velocity is kept constant. Under the condition, the effects of velocity change on temperature, net energy input, strain rate and material flow stress are studied. Their collective effects on dimension, residual stress, hardness and microstructure are also presented. Numerical results are experimentally validated and used to study process transiency, and aid understanding the complex and often conflicting effects of the condition.

Keywords: Laser forming; Line energy

1. Introduction

In laser forming, a laser is used to scan sheet metal material with a certain pattern so that the material deforms owing to thermal-induced distortion (Fig. 1). It is a flexible process, especially suitable for production of small-batch and high-variety sheet metal components, and prototypes [1]. Research on the laser forming process has intensified in recent years [2]. Examples include investigation on mechanisms [1], analytic modelling and numerical simulation [3–8], parametric analysis of influences of strain hardening [9], study of edge effects [10,11], working accuracy [12], and effects of strain rate [13].

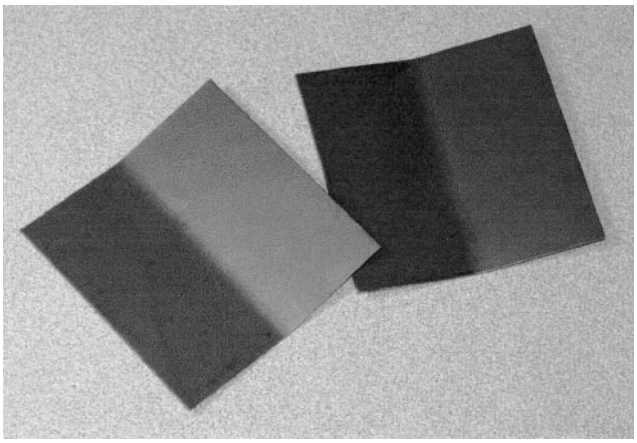

Fig. 1. Samples of straight-line laser forming (size, 80 × 80 × 0.89 mm^3).

Correspondence and offprint requests to: Dr Y. L. Yao, Department of Mechanical Engineering, Columbia University, 220 S. W. Mudd, Mail Code 4703, 500 West 120th Street, New York, NY 10027, USA. E-mail: ylyl@columbia.edu

In conducting these investigations, various experimental conditions were used. For example, deformations under different laser powers, scanning velocities or beam diameters were among the most commonly used conditions. Since the laser forming process is affected by many factors, it is sometimes advantageous to examine the effect of a combination of parameters. An example is the formation of the Fourier number, $F_o = \alpha_d d/s^2 V$, where α_d is the thermal diffusivity, d the beam diameter, s the sheet thickness, and V the scanning velocity. It has been shown that for a small Fourier number, the temperature gradient mechanism is more dominant, whereas for a large Fourier number, the buckling mechanism is more dominant. It is obvious that a single parameter would not do what the Fourier number does, that is, to serve conveniently as a measure for difficult forming mechanisms.

Another combination of process parameters has been the line energy (LE), which is defined as $LE = P/V$, where P is the laser power and V is the scanning velocity. The unit of line energy is J/m^{-1} when the units of P and V are W and m s^{-1}. Line energy represents the laser energy input per unit length along the scanning path. It makes sense to consider the parameters in this way because P is laser energy generation per unit time while V affects laser energy input to workpiece per unit time. It is convenient, for example, to specify a different value of line energy for a different material or sheet thickness. It is, however, easy to assume that if the line energy is held constant, the forming results will be identical for identical material and geometry. This has been shown not to be the case. For example, Magee, et al. [10,14] have carried out experiments under the condition of constant line energy. When the scanning velocity (as well as the laser power) increases proportionally, the bend angle increases before it levels off. This indicates that, although the line energy seems to be a useful measure in laser forming, a better understanding of the underlying implications, when the line energy is held

constant while velocity and power change, will ensure appropriate use of the measure in laser forming.

This paper briefly analyses the physical phenomena taking place when line energy is held constant while velocity and power change, and experimental details are given. To help understand the transient conditions, a numerical simulation is carried out, which is validated by the experimental results.

2. Constant Line Energy

In laser forming under the condition of constant line energy, the line energy, that is, the ratio between laser power P and scanning velocity V is kept constant, while P and V may vary proportionally. When this happens, the heat dissipation rate and strain rate will change and result in deformation, or the microstructure may change, despite the fact that the laser energy input length along the scanning path is kept constant.

Heat has less time to conduct at a higher velocity. As a result, the temperature at a higher velocity is higher than that at a lower velocity, despite a higher laser power. This has a number of implications. It increases the radiation loss to the surroundings because the radiation is strongly dependent on temperature. However, the radiation loss is much smaller than the conductive loss because only a very small surface is heated in laser forming. Therefore, the total heat dissipation at a higher velocity is smaller than that at a lower velocity (which will be shown later). Convective loss is not considered in our study because no gas or liquid jets are used for cooling.

Secondly, the higher temperature at the higher velocity has a conflicting effect on the material flow stress. Flow stress decreases as temperature increases but increases with strain rate. Furthermore the increased temperature makes the effect of strain rate on flow stress more pronounced. The net effect of the higher velocity on flow stress therefore cannot be readily predicted and requires more investigation. As a result, the dimensions and residual stress of formed parts will be different even under conditions of constant line energy.

The difference in temperature and strain rate at different velocities may also affect the hardness and microstructure of formed parts. Changes in flow stress can be empirically linked to changes in hardness. High temperature and more deformation may lead to recrystallisation of formed parts.

3. Experiment

The samples were made from low carbon steel AISI 1010. The length of the samples is 76~80 mm, the width is 40 mm, and the thickness is 0.89~1.5 mm. Laser scanning takes place along the direction of width. The samples were cleaned using propanol followed by graphite coating to increase the coupling of laser power. The bending of the samples was measured using a coordinate measuring machine at 3 to 5 locations along the scanning path and their average was calculated. The laser system used for laser forming was a PRC1500 CO_2 laser system. Its maximum power was 1.5KW, and power density distribution was TEM_{00}. The diameter of the laser beam is the diameter at which the power density becomes $1/e^2$ of the maximum value. Laser beam diameter varies from 2 to 4 mm by varying the distance between the focus lens and the top surface of the workpiece. In the experiment, the X-axis is defined as the direction of the scanning path, the Z-axis as the thickness direction, and the Y-axis as the direction perpendicular to the X- and Z-axes. The experimental conditions are listed in Table 1. For microstructure observation, samples were etched using 3% HNO_3 for 20 s and observation was carried out using a scanning electron microscope.

4. Numerical Simulation

Numerical simulation of the laser forming process was realised by a finite-element method (FEM). The Code ABAQUS version 5.7 was used for this work. The simulation conditions correspond with the experimental conditions. For convenience, the same mesh model is used for thermal and structural analyses. A 3D element with 20 nodes was used instead of an 8-node element, since it has no shear locking and hourglass stiffness. To specify the Gaussian distribution of laser beam intensity, a user-defined FORTRAN program was written to interface with the exiting code. The output of the FEM numerical simulation includes the spatial and temporal distribution of temperature, stress, and elastic and plastic strains.

The following main assumptions are used in the numerical simulation. The total strain, $d\epsilon$, is composed of elastic, plastic, creep, and thermal strains, $d\epsilon^{el}$, $d\epsilon^{pl}$, $d\epsilon^{c}$, and $d\epsilon^{th}$. Because the time involved in the laser forming process is very short, the third term $d\epsilon^{c}$ was neglected.

Plastic deformation energy is neglected because it is much smaller than the laser input in the laser forming. The deformation temperature is lower than the melting temperature of the workpiece material. The workpiece is continuous and isotropic.

In the numerical simulation, the boundary conditions are as follows. A symmetric plane is one corresponding to the scanning path (X, Z-plane). Owing to its symmetry, the plane is

Table 1. The experimental conditions.

LE	d=2 mm	d=3 mm	d=4 mm
5 J mm^{-1}	V=10–290 mm s^{-1} P=50–1450 W	V=10–270 mm s^{-1} P=50–1350 W	V=10–280 mm s^{-1} P=50–1400 W
7.5 J mm^{-1}		V=53.3–180 mm s^{-1} P=400–1350 W	
10 J mm^{-1}			V=40–138 mm s^{-1} P=400–1380 W
15 J mm^{-1}			V=13.3–90 mm s^{-1} P=200–1350 W
20 J mm^{-1}			V=2.5–67.5 mm s^{-1} P=50–1350 W
30 J mm^{-1}			V=13–47 mm s^{-1} P=390–1410 W

(Workpiece size: 76×40×1.5 mm^3 for the last condition, 80×40×0.89 mm^3 for all other conditions, *LE*: line energy, *d*: diameter, *V*: velocity, *P*: power.)

an adiabatic surface, and no movement of material takes place across it. The surfaces of the workpiece undergo free convective heat transfer with the atmosphere except at the top surface where there is a low gas flow coaxial with the laser beam for lens protection. Surface convective heat flux is $f=h(T - T_s)$, where h is the convective heat transfer coefficient, T the surface temperature, and T_s the surrounding temperature. The radiation heat flux is $f=A(T^4 - T_s^4)$, where A is the radiation constant.

For mechanical analysis, Hooke's law was used for elastic deformation and the flow rule, which relates strain to stress for plastic deformation is written as $d\epsilon_{ij} = d\lambda\ (\partial f/d\sigma_{ij})$ where σ is the stress, ϵ is the strain, $d\lambda$ is the instantaneous, positive, varying, proportionality factor (plastic compliance), and $f = f(\sigma_{ij})$ describing yielding. In this simulation, Von Mises' criterion was used, which postulates that, when the root-mean shear stress reaches a constant, yielding of the material will take place. As Von Mises' criterion is used, the following equation can be obtained for an isotropic material

$$\frac{d\epsilon_x}{\sigma_x - \sigma_m} = \frac{d\epsilon_y}{\sigma_y - \sigma_m} = \frac{d\epsilon_z}{\sigma_z - \sigma_m} = \frac{d\gamma_{xy}}{2\tau_{xy}} = \frac{d\gamma_{yz}}{2\tau_{yz}} = \frac{d\gamma_{zx}}{2\tau_{zx}} = d\lambda$$

where σ_m is the mean or hydrostatic stress, τ is the shear stress, and γ is the shear strain.

Workhardening of the workpiece was considered, that is, when plastic deformation occurs, $\sigma = K\epsilon^n$ where K is the strength coefficient, and n is the strain-hardening exponent. The influence of the strain rate on the flow stress of the material is also taken into consideration in the simulation, that is, the flow stress, σ, relates to the strain rate, $\dot{\epsilon}$, as $\sigma = C\dot{\epsilon}^m$ where C is the strength coefficient, and m is the strain rate sensitivity exponent. It should be noted that m increases with temperature. In the numerical simulation process, m for the low carbon steel, at different temperatures, was first obtained by the procedure outlined in [12]. The effects of strain rate were then simulated by inputting r values obtained from the m values at different temperatures and strain rates. r is defined as $r = \sigma/\sigma_s$, where σ is the flow stress at different strain rates and temperatures, and σ_s is the static flow stress.

5. Results and Discussion

The dependence of bend angle on scanning speed is shown in Fig. 2 for a beam diameter of 2, 3, and 4 mm. The line energy for each curve is kept constant while path feedrate increases. At a lower velocity, though the thickness temperature gradient is smaller, the difference of thermally induced distortions between the top and bottom surfaces is smaller, and heat dissipation has time to take place. As a result, the bend angle remains small at the lower velocity. In the higher velocity region, it can be seen that, when the diameter of the laser beam decreases, the slope of the curve decreases, and the bend angle in the case of 2 mm diameter decreases with increasing velocity. The phenomena can be explained as follows. The ratio r between the real flow stress at different strain rates and static flow stresses changes with temperature, as shown in Fig. 3. At a high temperature, the increment of the ratio for a certain strain rate increment is higher than that at a low

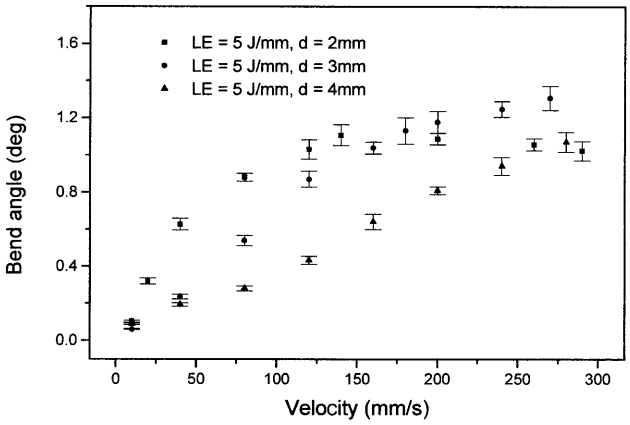

Fig. 2. Bend angle vs. scanning velocity with different beam diameter d (*LE*, line energy held constant; size, 80 × 40 × 0.89 mm^3).

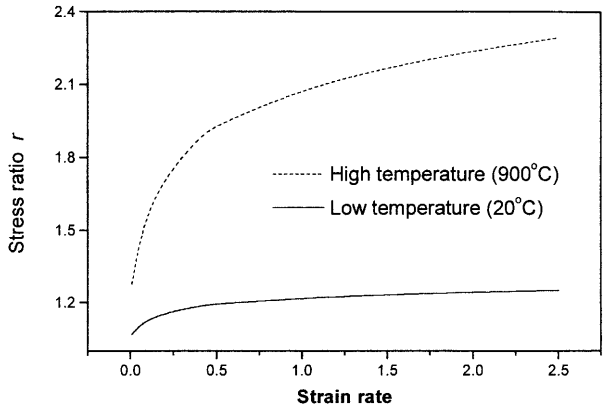

Fig. 3. Typical relationship between the stress ratio (real flow stress vs. static flow stress) and strain rate at different temperatures.

temperature. Static flow stress generally decreases with increasing temperature and the rate of decrease increases with temperature. Therefore, at a higher temperature, the stress change caused by strain rate change is more significant. For the cases shown in Fig. 2, although the temperature tends to rise, the flow stress tends to drop as beam diameter decreases, the increased strain rate accompanying the increased velocity affects the flow stress more significantly. As a result, the bend angle for the small beam diameter at higher velocities tends to level off or even decrease.

Figure 4 shows the relationship between bend angle and scanning speed for samples scanned at different line energies of 10, 15, and 20 mm s^{-1} with the same beam diameter of 4 mm. The higher the line energy, the larger the bend angle. When the line energy is higher, the slope of the curve increases faster because the higher line energy corresponds to a high temperature which makes the influence of strain rate on flow stress more pronounced.

In order to describe the energy input by a laser beam to a sample, per unit area, a term, called *area energy*, is defined as $AE = P/Vd = LE/d$, where P is the power of the laser beam, V the scanning velocity, and d the diameter of the laser beam. When the units of P, V and d are W, m s^{-1}, and m, the unit of the area energy is J m^{-2}. The area energy is a

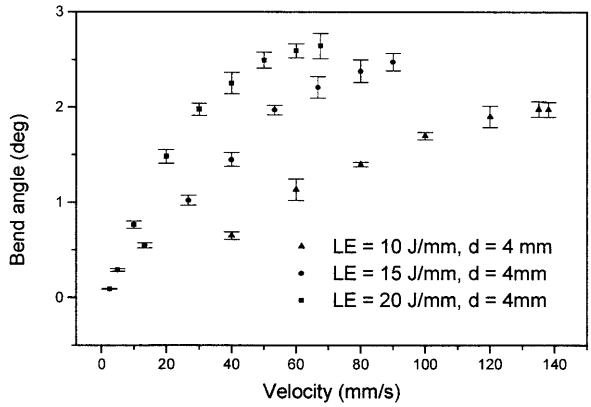

Fig. 4. Bend angle vs. scanning velocity with different line energy *LE* (*d*, beam diameter held constant; size, 80 × 40 × 0.89 mm^3).

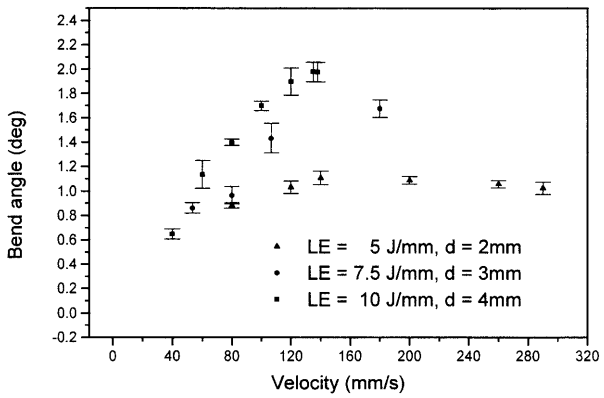

Fig. 5. Bend angle vs. scanning velocity under the condition of constant area energy (*LE*, line energy; *d*, beam diameter; size, 80 × 40 × 0.89 mm^3).

measure of the average energy applied to unit area along the laser scanning path, because the intensity of the laser beam normally has a Gaussian distribution.

Using the area energy concept, the laser forming processes, with different line energies and laser beam diameters, can be compared to find the bending characteristics with the same area energy. Three curves in Fig. 5 have different line energies and beam diameters, but every point has an identical area energy, 2.5 J mm^{-2}. It can be seen from Fig. 5 that the bend angle is larger when the line energy is higher and the beam diameter is larger because in this case more energy is put in despite the area energy being the same as for the others. This leads to the calculation of the bend angle per unit width of the scanning path (Fig. 6). Dividing the bend angle by the beam diameter and then plotting it against the velocity shows identical curves for different line energies and laser beam diameters, as long as the average energy input by the laser beam per unit area is the same.

Figure 7 shows comparisons of experimental and simulation results under typical conditions. Figure 7(*a*) is for scanning at a line energy of 10 J mm^{-1} and a beam diameter of 4 mm. The dimensions of the workpiece are 80 × 40 × 0.89 mm^3. Figure 7(*b*) is for samples whose size is 76 × 40 × 1.5 mm^3, for a line energy of 30 J mm^{-1} and a beam diameter of 4 mm.

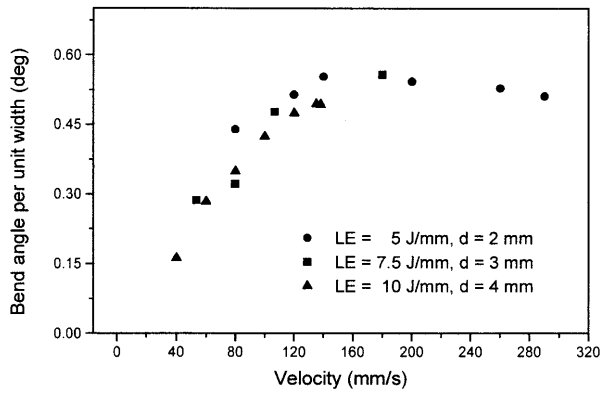

Fig. 6. Bend angle per unit width of scanned area vs. velocity (*LE*, line energy; *d*, beam diameter; size, 80 × 40 × 0.89 mm^3).

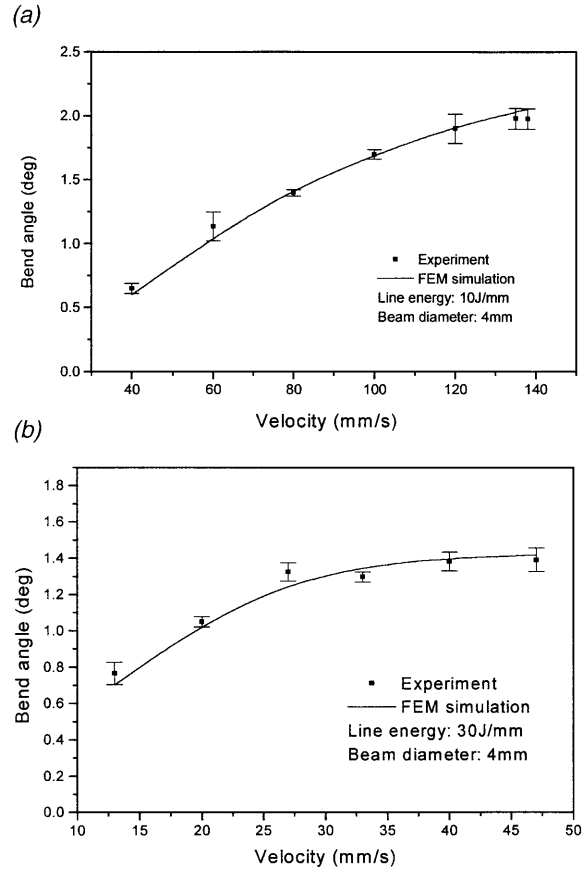

Fig. 7. Comparison of simulation and experimental results under typical conditions (*a*) 80 × 40 × 0.89 mm^3, (*b*) 76 × 40 × 1.5 mm^3.

It can be seen that the simulation results agree well with the experimental results which therefore validates the numerical simulation results.

Figure 8 shows a typical simulation result of the time history of the *Y*-axis plastic strain at the top and bottom surfaces on the scanning path (to which the *Y*-axis is perpendicular and the *Y*-axis is within the workpiece). The average plastic strain in the *Y*-direction along the scanning path is shown in Fig. 9. The plastic strain on the upper surface is compressive and that

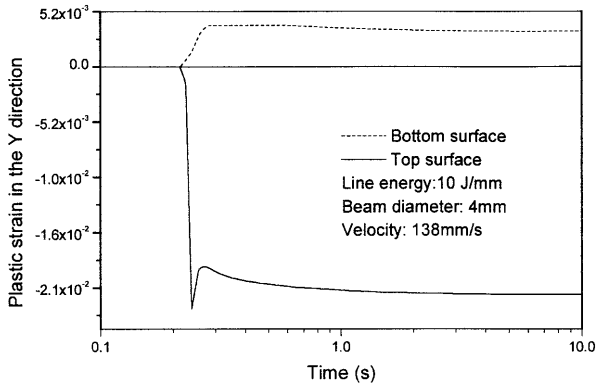

Fig. 8. Typical simulation result of time history of plastic strain (size, 80 × 40 × 0.89 mm³).

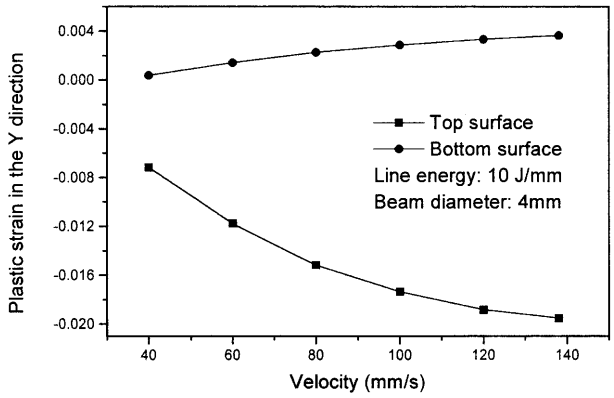

Fig. 9. Variation of plastic strain with velocity (simulation results; size, 80 × 40 × 0.89 mm³).

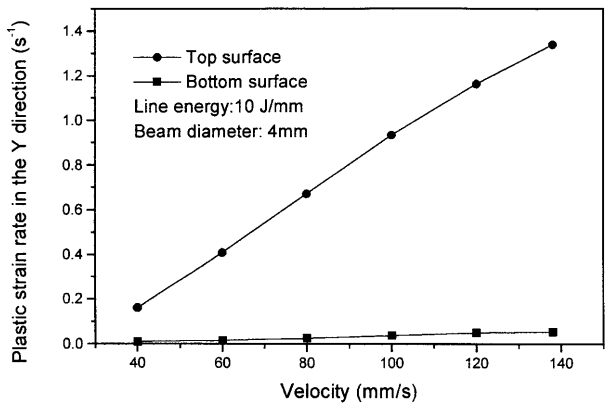

Fig. 10. Simulation result of strain rate vs. scanning velocity (size, 80 × 40 × 0.89 mm³).

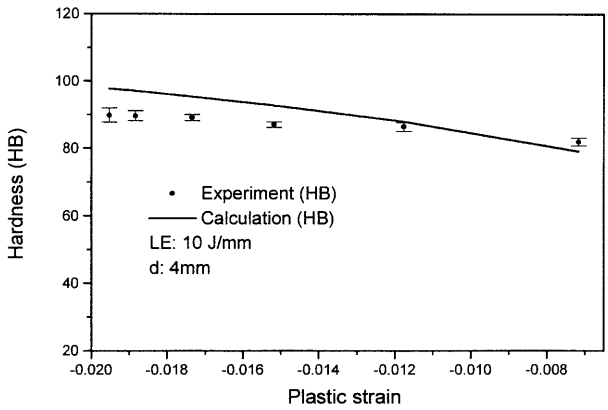

Fig. 11. Hardness measurement vs. plastic strain (size 80 × 40 × 0.89 mm³).

on the lower surface is tensile. These results can be easily understood. A laser scan forms a steep thermal gradient through the workpiece thickness and so the top surface has a much larger tendency to expand thermally, but the surrounding material restricts the expansion. With continued heating by the laser beam, the material flow stress decreases, and further thermal expansion results in plastic compression at the top surface. At the cooling stage, the material that has been compressed in the upper layers contracts so that a shortening of these layers makes the sample bend towards the laser. As a result, there is a compressive deformation in the upper layers, and a tensile deformation in the lower layers. When the laser scanning velocity increases, the temperature of the heat affected zone increases, which makes the thermal expansion larger and the flow stress lower so that the plastic deformation becomes larger. Figure 10 shows the dependence of the plastic strain rate in the *Y*-direction on the scanning velocity. It can be seen that the strain rate is almost directly proportional to the velocity, and the strain rate increases significantly at the top surface, and changes little at the bottom surface.

Figure 11 shows the relationship between hardness at the upper surface of the scanned parts and the plastic strain. When the velocity increases, the absolute value of the plastic strain on the top surface increases, as shown in Fig. 9. Owing to work hardening, the flow stress of the parts increases and the hardness increases. The hardness is calculated as follows. By substituting the plastic strain and the strain-hardening exponent for the material in $\sigma = K\epsilon^n$, the stress can be calculated. Using the well-known empirical relationship between the hardness and the stress for steel, the hardness can be obtained. From the figure, it can be seen that for smaller compressive plastic strain values, which correspond lower velocities, the calculated results agree with experimental observation, but for larger compressive strains, the calculated values are a little higher. This is because at high strains (also higher temperature), recrystallisation and dissolution of hard particles take place, which typically reduce hardness. This will be further explained later in the section.

Temperature histories on the top and bottom surfaces along the scanning path are presented in Fig. 12. It is seen that at a lower scanning velocity, the maximum temperature is lower. As mentioned earlier, this is due to the fact that there is more time for heat transfer to the surrounding material than at a higher velocity. The temperature difference between the top and bottom surfaces is also smaller at a lower velocity for the same reason.

Figure 13 shows the residual stress on the upper and lower surfaces in the *Y*-direction. As the speed is very low, the temperature of the heated area is low and so is the thermal expansion of the materials. The reduced local shortening leads

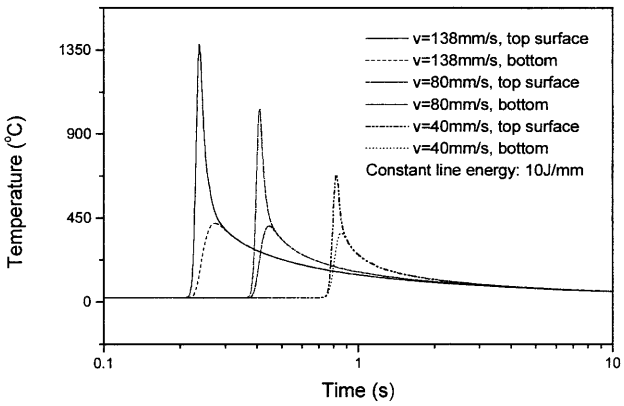

Fig. 12. Variation of the temperature on the top and bottom surface with time (size, 80 × 40 × 0.89 mm^3).

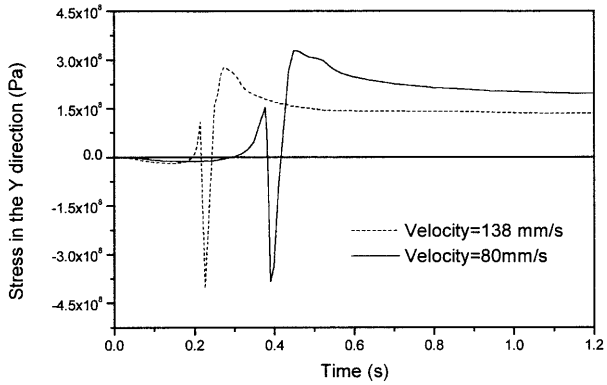

Fig. 14. The time history of stresses on the top surface for the samples scanned at different velocities (line energy, 10 J mm^{-1}; beam diameter, 4 mm; size, 80 × 40 × 0.89 mm^3).

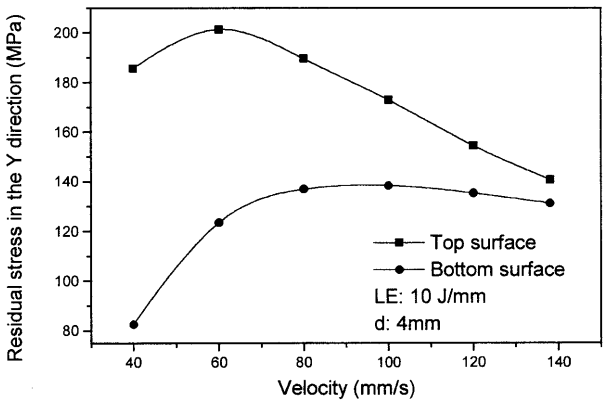

Fig. 13. Variation of residual stresses with velocity (size, 80 × 40 × 0.89 mm^3).

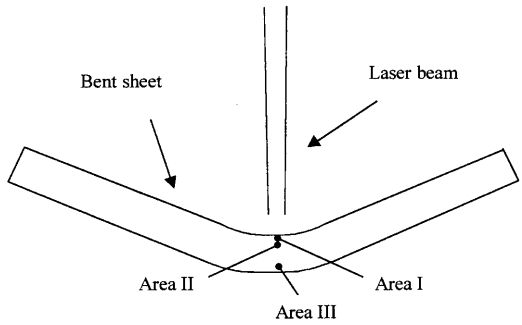

Fig. 15. Areas where SEM micrographs were taken.

to small residual stresses. Figure 14 compares the time history of stress at the velocities of 80 and 138 mm s^{-1}. At the beginning of deformation, the stress becomes tensile owing to the expansion of the immediately preceding material. At low velocity, the temperature is low and the flow stress associated with it is high. Therefore, the stress is higher than that at high velocity. The increase of stress beyond the minimum value results from the thermal expansion of the material immediately after the current location. For the same reason, the stress rise is higher at lower velocity. As a result, the residual stresses are lower for the sample scanned at higher velocity than at the lower velocity.

The microstructure of the samples scanned at each velocity was examined and Fig. 15 shows the three areas where the scanning electron micrographs were taken. Figure 16(*a*) shows the microstructure of the low carbon steel material as received. The darker background is ferrite. The lighter-coloured particles are likely to be carbide. Figures 16(*b*), 16(*c*), and 16(*d*) are the microstructures of a workpiece scanned at a velocity of 138 mm s^{-1} in the areas I, II, and III. In area I, the size of the grains becomes markedly smaller. This is because, owing to the high deformation and temperature involved, recrystallisation of material has taken place there. Grain refinement has a number of beneficial effects on material properties in service. In the zone near the upper surface, that is, areas I and II, most carbide particles are dissolved owing to higher temperature (Figs. 16(*b*) and (*c*). In the area near the bottom surface, that is, area III (Fig.16(*d*)), no grain refinement is seen, and the density of the particles is unchanged because the temperature and deformation there are lower. For a sample scanned at a low velocity, such as 40 mm s^{-1} (Figs. 16(*e*) and 16 (*f*)), recrystallisation and dissolution are not found, and the number of the particles remains unchanged in both areas I and III. This is because both temperature and deformation at the lower velocity are lower.

The recrystallisation can reduce the influence of work hardening. The dissolution of particles also reduces material strength. Both factors can reduce the hardness of the material. In the calculation of the hardness (see Fig. 11), these factors are not considered, so the calculated values are higher than the measured ones in the higher compressive strain region.

6. Conclusions

The laser forming process, with constant line energy, was investigated experimentally and numerically. Under the condition of constant line energy, the bend angle increases with scanning velocity, but the degree of increase reduces

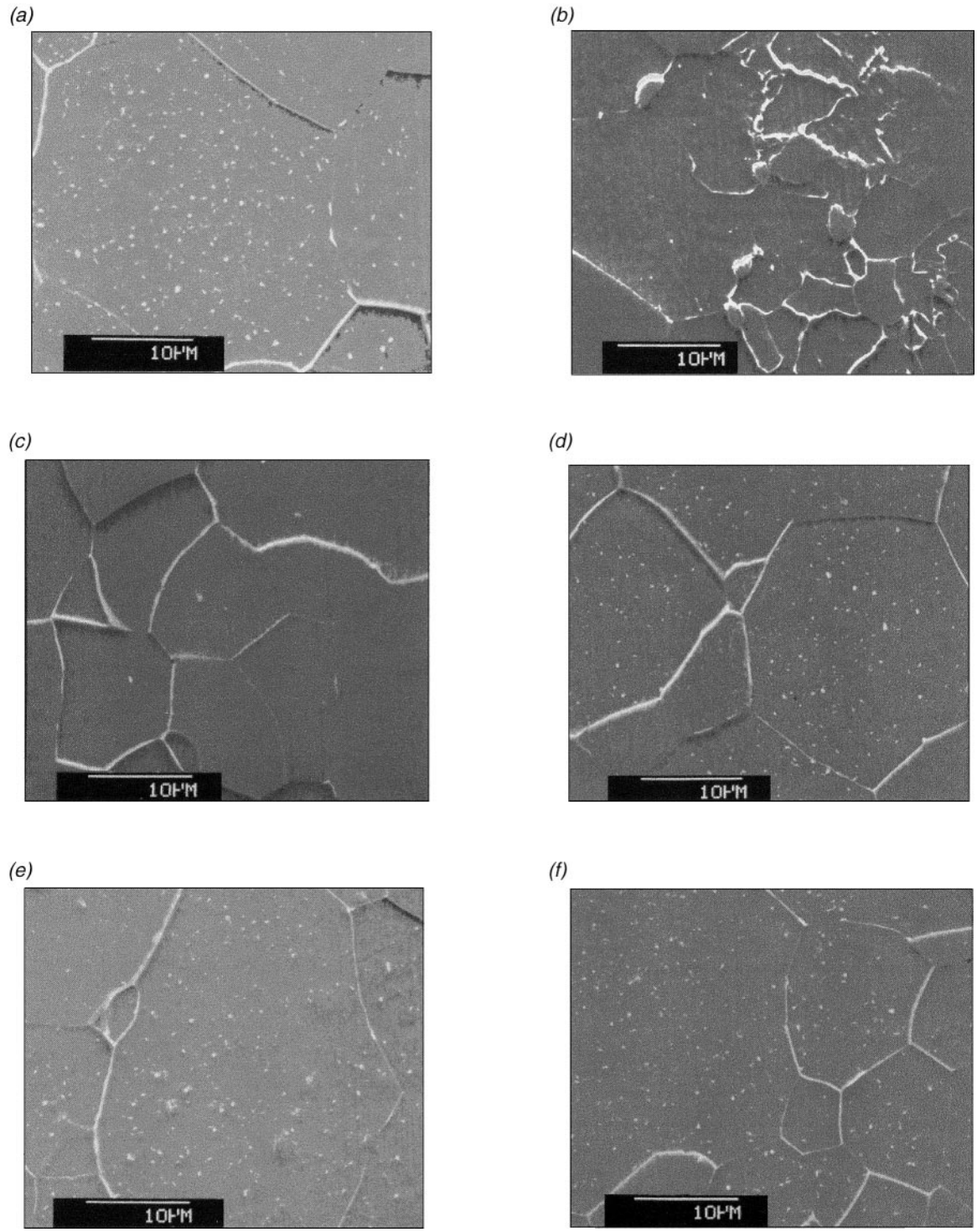

Fig. 16. SEM micrographs of the microstructure of AISI 1010 before and after laser forming (line energy, 10 J mm^{-1}; beam diameter, 4 mm). (*a*) As received. (*b*) Area I after high strain rate *LF* (v = 138 mm s^{-1}). (*c*) Area II after high strain rate *LF* (v = 138 mm s^{-1}). (*d*) Area III after high strain rate *LF* (v = 138 mm s^{-1}). (*e*) Area I after low strain rate *LF* (v = 40 mm s^{-1}). (*f*) Area III after low strain rate *LF* (v = 40 mm s^{-1}).

with velocity increase. When the velocity is high, the strain rate is high, causing flow stress to increase. At the same time, the temperature rises owing to less heat dissipation, which causes the flow stress to reduce. However, at elevated temperatures, the influence of strain rate on the flow stress is more significant, causing the net flow stress to rise and the bending angle increase to slow down. With the scanning velocity increase, the hardness of formed samples increases,

mainly owing to work hardening. When low carbon steel parts are formed at high velocity, recrystallisation and dissolution of hard particles occurs owing to the high temperature and deformation. In conclusion, under the condition of constant line energy, process results can be different and thus the employment of constant line energy must be undertaken cautiously.

Acknowledgements

The authors gratefully acknowledge Mr J. Bao for his assistance in the numerical simulation, and Mr Jack Tsai and Ms Dee Berger for their assistance in scanning electron microscope observations.

References

1. F. Vollertsen, "Mechanism and models for laser forming", Laser Assisted Net Shape Engineering, Proceedings of the LANE'94, vol. 1, pp. 345–360, 1994.
2. J. Magee, K. G. Watkins and W. M. Steen, "Advances in laser forming", Journal of Laser Application, 10, pp. 235–246, 1998.
3. F. Vollertsen, M. Geiger and W. M. Li, "FDM and FEM simulation of laser forming a comparative study", Advanced Technology of Plasticity, 3, pp. 1793–1798, 1993.
4. F. Vollertsen, "An analytical model for laser bending", Laser in Engineering, 2, pp. 261–276, 1994.
5. Y.-C. Hsiao, H. Shimizu, L. Firth et al. "Finite element modeling of laser forming", Section A-ICALEO 1997, pp. 31–40, 1997.
6. N. Alberti, L. Fratini and F. Micari, "Numerical simulation of the laser bending process *b a* coupled thermal mechanical analysis", Laser Assisted Net Shape Engineering, Proceedings of the LANE'94, vol. 1, pp. 327–336, 1994.
7. N. Alberti, L. Fratini, and F. Micari et al. "Computer aided engineering of a laser assisted bending process", Laser Assisted Net Shape Engineering 2, Proceedings of the LANE'97, vol. 2, pp. 375–382, 1997.
8. T. B. Kermanidis, A. K. Kyrsanidis and S. G. Pantelakis, "Numerical simulation of the laser forming process in metallic plates", Proceedings of the International Conference on Computer Methods and Experimental Measurements for Surface Treatment Effects, pp. 307–316, 1997.
9. A. Sprenger, F. Vollertsen, W. M. Steen et al. "Influence of strain hardening on laser bending," Laser Assisted Net Shape Engineering, Proceedings of the LANE'94, vol. 1, pp. 361–370, 1994.
10. J. Magee, K. G. Watkins and W. M. Steen, "Edge effects in laser forming", Laser Assisted Net Shape Engineering 2, Proceedings of the LANE'97, Meisenbach Bamberg, pp. 399–406, 1997.
11. J. Bao and Y. L. Yao, "Analysis and Prediction of Edge Effects in Laser Bending", Proc. 18th ICALEO, San Diego, CA, section C, pp. 186–195, Nov. 1999.
12. T. Hennige, S. Holtzer, F. Vollertsen and M. Geiger, "On the working accuracy of laser bending", Journal of Materials Processing Technology, 71, pp. 422–432, 1997.
13. W. Li and Y. L. Yao, "Effects of Strain Rate in Laser Forming", Proc. 18th ICALEO, San Diego, CA, section F, pp. 107–106, Nov. 1999.
14. J. Magee, K. G. Watkins and W. M. Steen, "Laser forming of aerospace alloys", Section E-ICALEO 1997, pp. 156–165, 1997.